Wound-triggered Shape Change Microgels for the Development of Enhanced Biomimetic Function Platelet-like Particles

Eunice Chee, PhD[1,2], Emily Mihalko, PhD[3], Kimberly Nellenbach, PhD[1,2], Jennifer Sollinger[1], Ke Huang, MD, PhD[4], Mason Hon[1], Sanika Pandit[1,2], Ke Cheng, PhD[4], Ashley Brown, PhD*[1,2]

[1]Joint Department of Biomedical Engineering of North Carolina State University and University of North Carolina – Chapel Hill, Raleigh, NC, 27606
[2]Comparative Medicine Institute, North Carolina State University, Raleigh, NC 27606
[3]Trauma and Transfusion Medicine Research Center, University of Pittsburgh, Pittsburgh, PA 15213
[4]Department of Molecular Biomedical Sciences, North Carolina State University, Raleigh, NC 27607

*Corresponding Author: Ashley C. Brown, PhD
Address: Joint Department of Biomedical Engineering
North Carolina State University and University of North Carolina at Chapel-Hill
1001 William Moore Dr., Raleigh, NC, 27606
Phone: (919) 513-8231
Email: aecarso2@ncsu.edu

Keywords: wound healing, synthetic platelet, hemostasis, fibrin, trauma

Abstract:

Platelets play a pivotal role in hemostasis and wound healing and conditional shape change is an important component of platelet functionality. In normal circumstances, platelets travel through the circulatory system in an inactive rounded state, which enables platelets to easily move to vessel walls for attachment. When an injury occurs, platelets are prompted by molecules, such as thrombin, to shift into a stellate shape and increase exposure of fibrin-binding receptors. When active, platelets promote hemostasis and clot retraction, which enhances clot stability and promotes healing. However, in conditions where platelets are depleted or hyporeactive, these functions are diminished and lead to inhibited hemostasis and healing. To treat platelet depletion, our group developed platelet-like particles (PLPs) which consist of highly deformable microgels coupled to fibrin binding motif. However, first generation PLPs do not exhibit wound-triggered shape change like native platelets. Thus, the objective of these studies was to develop a PLP formulation that changes shape when prompted by thrombin. To create thrombin-sensitive PLPs (TS-PLPs), we incorporated a thrombin-cleavable peptide into the microgel body and then evaluated PLP properties before and after exposure to thrombin including morphology, size, and *in vitro* clot retraction. Once thrombin-prompted shape change ability was confirmed, the TS-PLPs were tested *in vivo* for hemostatic ability and subsequent wound healing outcomes in a murine liver trauma model. We found that TS-PLPs exhibit a wound-triggered shape change, induce significant clot retraction following exposure to thrombin and promote hemostasis and healing *in vivo* after trauma.

Introduction:

Under normal circumstances, platelets circulate in a round, inactive state in the circulatory system. In this state, platelets can easily marginate or move to the vessel wall for attachment. When injury occurs, platelets are prompted by injury-associated molecules, including thrombin, to shift into a stellate shape and increase surface exposure of fibrin-binding receptors. In this activated state, platelets can mediate the hemostatic process through platelet aggregation during primary hemostasis and promotion of fibrin formation during secondary hemostasis. After the formation of a fibrin-rich clot, platelets utilize actin-myosin machinery to pull on the fibrin network, resulting in clot retraction (1, 2). Retracted clots have increased stiffness compared to unretracted clots, which enhances clot stability. Additionally, newer evidence suggests that increased stiffness due to clot retraction may contribute to healing after cessation of bleeding by guiding cells into the wound bed by durotaxis.

In conditions where platelets are depleted or hyporeactive, such as trauma, surgical associated bleeding, or chronic wounds, platelets are unable to carry about their functions, leading to inhibited hemostasis and wound healing (3). Such situations are prevalent and represent a pressing clinical need. For example, traumatic injury remains the leading cause of death for people under the age of 45 (4). Furthermore, chronic wounds frequently affect diabetic patients and 34.2 million diabetic patients are in the United States alone (5).

To address the consequences of platelet depletion or hyporeactivity, many platelet-mimetic strategies have been investigated. Platelet derived strategies are based on using substances derived from natural platelets and include platelet transfusions and lyophilized platelets. However, these strategies have extremely short storage lifetimes (6, 7) and can lead to immunogenicity issues (8, 9) due to their origins from allogeneic sources. As an alternative to natural platelet transfusions,

artificial platelets have been a key area of development in recent years. Artificial platelets designs include particles or polymers coupled to bioactive motifs such as RGD peptides or antibodies that bind to platelets or coagulation factors (10-12). While the synthetic nature of these strategies allows for longer storage lifetimes and easier scale up, artificial platelet strategies rarely mimic more than one platelet function (13). Cloaking and active delivery strategies have also been investigated. These approaches consist of coupling drug delivery vessels to platelet binding motifs or platelet membranes (14). While this construction allows for enhanced targeted delivery and reduced immune response when compared to uncloaked drug delivery, it requires the extraction of components from pre-existing platelets, which are not easily obtained or transported.

As a treatment for the effects of platelet depletion, our group has developed synthetic platelet-like particles (PLPs) consisting of a microgel coupled to a fibrin-targeting antibody (15). Previous work in our group has demonstrated that a highly deformable microgel is mimetic of active platelet morphology and when combined with high fibrin targeting affinity, for example by coupling to a fibrin-targeting antibody, can recapitulate the clot retraction ability of natural platelets. As a result of this particle design, PLPs can hone specifically to injuries and enhance subsequent healing after cessation of bleeding. Previous work in our group has demonstrated that treatment by PLPs can lead to significantly reduced blood loss after traumatic injury and enhanced wound healing outcomes in full thickness dermal injuries (15, 16). The unique deformation properties of the PLPs combined with the high fibrin affinity are critical for the ability of the particles to induce clot retraction. PLP-mediated clot retraction occurs via a Brownian wrench mechanism in which highly deformable PLPs become bound to multiple fibrin fibers within a clot network and spread between the bound fibers. This enables the PLPs to exert a ‘pulling’ strain upon the bound fibers as the PLPs collapse back into a more energetically favorable conformation.

PLPs act as nucleation points throughout the clot network, and this 'pulling' action results in microscale collapses that propagate throughout the fibrin network to induce bulk clot contraction in a manner analogous to the actin- and myosin-driven clot contraction effected by platelets, though on a slower time scale than native platelet-mediated retraction.

While PLPs are a promising material towards addressing the problems that come with platelet depletion, they still lack the ability to mimic platelet shape change in response to injury cues. To that end, in this manuscript we describe the development of next generation PLPs that are amenable to change shape in response to thrombin found at the wound site (thrombin-sensitive PLPs, TS-PLPs). This work is inspired by our previous work where we created a shape-changing PLP design consisting of a CoreShell microgel architecture with a degradable core (17). In this prior design, the core particle consists of N-isopropylmethacrylamide (NIPMAM) crosslinked with N,N-(1,2-Dihydroxyethylene)bisacrylamide (DHEBA). The shell particle consists of poly(N -isopropylacrylamide) (pNIPAm) crosslinked with 2% N,N' - methylenebisacrylamide (BIS). Due to the DHEBA, the core degrades in the presence of sodium periodate (18-21). When the core of a CoreShell particle is degraded, it leaves behind a deformable hollow particle. Findings from this work showed that the CoreShell particle resembles inactive platelet morphology and the hollow particle resembles active platelet morphology (17). When coupled to fibrin-targeting antibody and incorporated into clots, it was found that intact CoreShell particles do not induce significant changes in clot structure while hollow particles do induce clot retraction, much like our base PLP technology. Additionally, when sodium periodate is added after incorporation of CoreShell particles into fibrin clots, the resulting clot structure was significantly more collapsed than control clot structure, demonstrating the potential for stimuli-responsive shape change (17). When applied to a full thickness dermal injury murine model, hollow particles were found to significantly

improve wound healing outcomes while CoreShell did not. This difference is consistent with the difference in deformability between the CoreShell and hollow particles. This prior work demonstrated the ability to induce a stimuli-responsive platelet-like shape change; however, sodium periodate is not a physiologically relevant, nor injury specific, stimuli.

Therefore, in this work we aimed to create a particle that would change shape in response to injury specific cues. Here we built upon our prior findings to develop a thrombin-sensitive nanogel (TSN) from NIPMAM crosslinked with a thrombin-cleavable peptide sequence (**Figure 1**), enabling the particle to change shape in the presence of thrombin (**Figure 2A**) In particular, we used the thrombin-sensitive peptide methacrylate-Gly-dPHe-Pro-Arg-Gly-Phe-Pro-Ala-Gly-Gly-Lys-methacrylate (22). We then evaluated morphology and size of the thrombin-sensitive nanogels in the absence or presence of thrombin using AFM (Atomic Force Microscopy), Nanosight, and cryoSEM (cryogenic Scanning Electron Microscopy). To evaluate clot retraction, all particle treatments were coupled to a polyclonal Fragment E anti-fibrin antibody and incorporated into clots. The resulting clots were then imaged by cryoSEM and analyzed for percent porosity. Finally, to evaluate *in vivo* hemostasis and wound healing, a murine liver laceration survival model was used. In the studies presented here, thrombin-sensitive PLPs (TS-PLPs) exposed to thrombin showed differences in morphology and clot retraction compared to non-exposed TS-PLPs. In addition, TS-PLPs demonstrated the ability to significantly stem bleeding in a traumatic injury model and significantly improve wound healing outcomes one week after injury.

Materials and Methods:

*Thrombin-sensitive Nanogel (TSN) Synthesis***:** To add thrombin sensitivity to nanogels, the custom peptide sequence methacrylate-Gly-dPHe-Pro-Arg-Gly-Phe-Pro-Ala-Gly-Gly-Lys-methacrylate (ordered from GenScript at >95% purity) was incorporated during microgel

synthesis. While stirred at 450 rpm, 85% NIPMAM and 5% thrombin-cleavable peptide were incubated in 95 mM TEMED and put under nitrogen purge for 1 hour at room temperature. 50 minutes into the purge, 10% Acrylic Acid was added. The reaction was then initiated at room temperature with 125 mM ammonium persulfate (APS) and allowed to react for 24 hours. The resulting reaction mixture was then purified by dialysis in ultrapure water in 1000 kDa dialysis tubing for 72 hours with water changes every 24 hours. The particle solution was then lyophilized and resuspended at desired concentrations with ultrapure water and stored at 4°C.

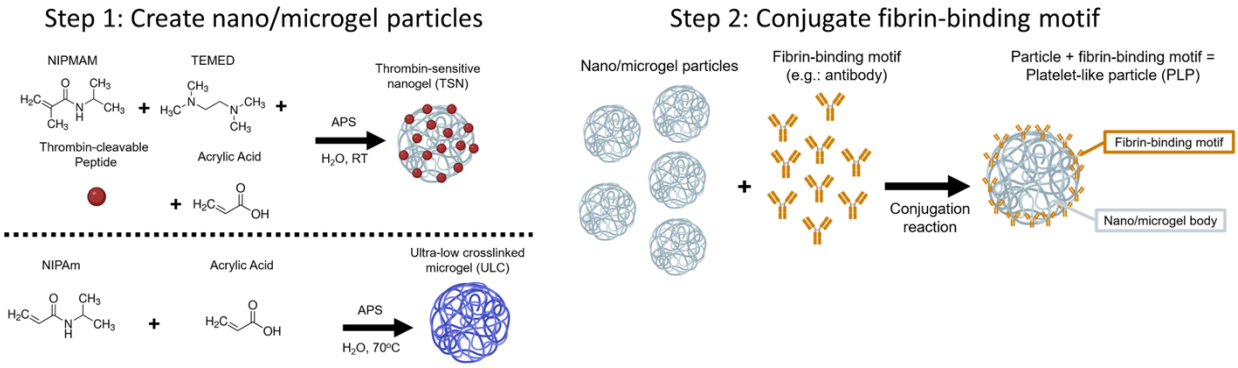

Figure 1: Overview of nanogel synthesis and fibrin-binding motif conjugation to create PLPs. Overview schematic of platelet-like particle fabrication. Creation of PLPs starts from fabrication of base nano/microgel particles through precipitation synthesis (Step 1). At this step, nano/microgel particles can be customized with different properties (e.g.: thrombin-sensitivity, crosslinker content and associated properties such as particle stiffness). Once base nano/microgel particles have been synthesized, they then become functionalized with fibrin binding ability through conjugation to a fibrin-binding motif via binding to acrylic acid groups by EDC/NHS chemistry (Step 2).

Size-matched Control Microgel Synthesis: To control for particle size effects, control microgels, size-matched to thrombin-sensitive nanogels, were synthesized via precipitation polymerization. Ultralow crosslinked microgels (ULCs) and 7% crosslinked BIS (7% BIS) were selected as highly deformable and nondeformable controls, respectively. ULCs consisted of 90% Poly(N-isopropylacrylamide) (NIPAm) and 10% Acrylic Acid (AAc) and 7% BIS particles consisted of 83% NIPAm, 10% AAc, and 7% N,N' - methylenebisacrylamide (BIS). A 100 mL

precipitation synthesis of 140 mM monomer solutions and varying amounts of SDS (4 mM for ULCs, 2 mM SDS for 7% BIS) were filtered through a 0.2 μm filter with AAc added 10 minutes prior to the addition of 1 mM ammonium persulfate (APS). The mixture was then allowed to react for 6 hours at 70°C flux with nitrogen purge. Resulting product solutions were then allowed to cool to room temperature and filtered against glass wool. Dialysis in 1000 kDa tubing against water was then conducted for 48 hours with 2 hour water changes for the latter 24 hours. The purified particle solutions were then frozen, lyophilized and resuspended at desired concentrations.

Particle Size Characterization: Dilutions of particle solutions were analyzed on a Malvern NanoSight NS300 for hydrodynamic radius characterization with size and distribution determined from 10 measurements of 30 seconds or 5 measurements of 60 seconds. Particle size and morphology was also analyzed via atomic force microscopy (AFM) imaging. For AFM imaging, cover glass was cleaned by sonication in a sequence of solutions for 10 minutes per solution. The sequence of solutions is as follows: Alconox, deionized water, acetone, ethanol (200 proof), and isopropyl alcohol. 50 μL of particle suspension was then deposited onto cleaned cover glass and allowed to air-dry overnight. The cover glass is then mounted onto a microscope slide using epoxy. Air topography imaging was then conducted with a MFP 3D Bio AFM (Asylum). Topography and height trace images were then analyzed in ImageJ for particle diameter and height for at least 30 microgels per group.

Particle Morphology: Particle morphology was analyzed by cryogenic scanning electron microscopy (cryoSEM) on a JEOL 7600F with Gatan Alto and Horiba CL Detector at 5 kV acceleration beam. 10 μL of particle solutions were deposited into the sample holder and plunged into nitrogen slush. Samples were then fractured, sputtered with gold, and imaged.

Analysis of Thrombin-induced Degradation: Nanogel solutions were incubated with thrombin solutions for final thrombin concentrations of 50 U/mL or 75 U/mL and a final 0.5 mg/mL particle concentration for a total of 1 mL of solution. We evaluated two thrombin concentrations to determine the influence of thrombin concentration on degradation responses. We utilized 50 U/mL as our lowest thrombin concentration because pilot studies suggested that lower concentrations would be insufficient to induce rapid degradation. 100 μL time point aliquots were and analyzed for deformability, size and distribution, and morphology using AFM, Nanosight, and cryoSEM respectively. For AFM and Nanosight, aliquots were diluted 1:10 and analyzed as described in particle size characterization methods. For cryoSEM, a 1:4 dilution of TSNs in water to 100 U/mL thrombin was created with 50 μL timepoint aliquots collected for total volume 400 μL for a final particle concentration of ~1.2 mg/mL. Timepoints were as follows for AFM and Nanosight: t = 0, 2 hr, 4 hr, 24 hr, 48 hr, 96 hr, 1 wk. For cryoSEM, the timepoints were t = 0, 2 hr, 6 hr, 24 hr, 48 hr, 96 hr, 1 wk.

Analysis of Thrombin-sensitive Nanogel Penetration: To model the potential for thrombin to fully penetrate the thrombin-sensitive nanogels, nanogel solutions were lyophilized and then resuspended at 10 mg/mL in 5 μM 70 kDa FITC labeled dextran or 66 kDa FITC labeled bovine serum albumin (BSA). 70 kDa dextran and 66 kDa BSA were selected as model molecules, because their sizes are close to the molecular size of thrombin (72 kDa). After 24 hours, 10 μL of the suspension was deposited onto cleaned cover glass, allowed to dry, mounted to a microscope slide and then imaged on a LSM 880 confocal microscope. The resulting images were then analyzed by fluorescent trace on ImageJ.

Coupling of Anti-fibrin Antibody to Particles to Create Platelet-like-Particles (PLPs): To create PLPs, a sheep anti-fibrin Fragment E polyclonal antibody was coupled to the AAc groups

by EDC/NHS chemistry. PLPs refer to the products of the coupling of particles and Fragment E antibody. PLPs were purified by dialysis against diH_20 using 1,000 kDa dialysis tubing for 24 hours. The product was then lyophilized for 24-48 hours. PLP particles were then weighed and resuspended at 10 mg/ml. Products of anti-fibrin antibody coupling to particles are referred to as <particle type>-PLPs (e.g.: thrombin-sensitive nanogels conjugated to anti-fibrin Fragment E = thrombin-sensitive PLP).

Clot Retraction Analysis: Treatment clots were made of 2 mg/ml fibrin, 0.1 U/ml thrombin, 0.25 mg/ml of particles (TS-PLP, small ULC-PLP, small 7% BIS-PLP, or ULC-PLP) and 10% volume 10X HEPES buffer and allowed to polymerize for 48 hours. Control clots were created similarly without the presence of particles. All clots were made with total of 150 μL volume. 2 hours after initiation of polymerization, an overlay of 50 μL of 100 U/mL thrombin was added to clots. These studies utilized higher concentrations of thrombin than initial studies with particles in solution to account for the fact that thrombin would bind to fibrin. Clots were then imaged on a JEOL 7600F with Gatan Alto and Horiba CL Detector at 5 kV acceleration beam. 3 clots were imaged per group with at least three sites imaged per clot for analysis. Percent porosity for samples was determined using ImageJ.

In vivo Hemostatic and Wound Healing Evaluation: To evaluate *in vivo* hemostatic performance and wound healing outcomes, C57BL/6 mice were anesthetized with 2% isofluorane. All studies were conducted under approval by NCSU IACUC protocol. Treatments were administered by tail vein injection and allowed to circulate for 5 minutes. Treatment groups for this study were Saline, ULC-PLP, TS-PLP and 7% BIS-PLP. All PLP-based groups were administered intravenously at 100 μL of 5 mg PLPs/kg animal suspended in sterile saline. The liver of each mouse was then exposed. A liver laceration of 0.5 cm length was then made extending

from the apex of the exposed left lobe (**Figure 5A**) and blood was collected onto pre-weighed filter paper and parafilm. Bleeding over time was imaged at t=0, 30 s, 1 min, 2 min, 3 min, 4 min, and 5 min. At t=5 min, the filter paper and parafilm assembly was then measured. The liver was then returned to the abdomen and mice were aseptically sutured closed. Mice were then monitored daily for 1 week for body weight and signs of pain. After 1 week, mice were then sacrificed, and organs (wound site, healthy liver lobe, kidney, spleen, lungs, and heart) were harvested for histology.

Blood loss was evaluated by determining the weight of blood collected onto the filter paper and parafilm assembly and normalizing the resulting mass by the respective animal's body weight. To calculate bleeding over time, photos were taken at each of the listed time points (t=0, 30 s, 1 min, 2 min, 3 min, 4 min, and 5 min) and then calibrated to a ruler included in the photos for scale in ImageJ. The area where the blood had stained the filter paper was then measured by ImageJ. A separate study was conducted utilizing a terminal liver laceration model to determine particle presence immediately after injury. Injuries were performed on male C57/bl6 as described above and animals were sacrificed following the 5 minute bleeding period. Organs were harvested and prepared for histological analysis as described above.

Histological Analysis of Wound Healing Outcomes Following Liver Laceration: Histological analysis was conducted with hematoxylin & eosin (H&E) staining and immunofluorescent labeling for platelets, fibrin, particle treatments, and cell nuclei. To label platelets, monoclonal anti-integrin beta 3/CD61 SJ19-09 antibody from Novus Biologicals was used as primary antibody with secondary Alexa 594 antibody. To label fibrin, monoclonal UC45 was used as primary antibody with secondary Alexa 594 antibody. To label particle treatments, a polyclonal anti-sheep 488 FITC-conjugated secondary antibody was used, tagging the fibrin

specific antibody attached to particles. Cell nuclei were labeled by DAPI. Images were captured on an EVOS Auto FL microscope at 4x magnification for H&E stained wounds and 10x magnification for all other organs and fluorescently labeled wounds. For each fluorescently labeled wound, 3 images at different sites were taken.

To quantify wound healing outcomes, wound area and fluorescence thresholding area were measured on ImageJ. Wound area was measured from H&E stained sections. Total areas for fibrin, particle presence, and CD61+ expression were measured by conducting particle analysis on 8-bit images.

Histological Analysis of Off-target Effects: To quantify off-target effects and clotting, peripheral organ (healthy liver lobe, heart, lung, kidney, spleen) sections were fluorescently labeled for fibrin and particles using the same methods described for fluorescent labeling for wounds. Fibrin and particle presence were also quantified using the same methods.

Statistical Analysis: All statistical analysis was conducted in GraphPad Prism 9. Bleeding area vs. time data was analyzed by two-way ANOVA. All other data was analyzed with a one-way ANOVA. Normality testing via D'Agostino&Pearson was performed to determine appropriate post-hoc testing. In cases where sample size was insufficient for D'Agosino&Pearson, Shapiro-Wilk was used to test normality. For normally distributed data, a Tukey's posthoc test for multiple comparisons was used. For non-normally distributed data nonparametric one-way ANOVA by Kruskal-Wallis test with Dunn's post hoc test for multiple comparisons was used.

Results

Size Evaluation of Thrombin-sensitive Nanogels: Unmodified thrombin-sensitive nanogels were determined to have average dry diameter of 330±50 nm and average dry height of 33±10 nm. When imaged for morphology on cryoSEM, the thrombin-sensitive nanogels displayed a rounded

morphology. **(Figure 2)** When exposed to 50 U/mL or 75 U/mL thrombin, population distribution markers on Nanosight show significantly decreased size starting from t = 2 hr. However, size increased after 24 hours for samples exposed to 75 U/mL thrombin, potentially due to decreased crosslinking as thrombin cleaves the peptides; decreased crosslinking would then lead to increased swelling. AFM data with 50 U/mL thrombin shows no significant changes in particle diameter until t=2 hr, 24 hr and 96 hr, compared to t=0 particle diameter. In the presence of 50 U/ml thrombin, particle height also significantly decreased starting from t=24 hr, compared to t=0 particle height. Taken together, these findings indicate that particle deformability significantly increases t=24 hr after exposure to thrombin (**Supplemental Figure 1**). Size increases in solution at later time points, in combination with decreasing particle height observed via AFM images of dried particles, may indicate swelling and increased deformability due to decreased particle crosslinking after thrombin cleavage of the peptide. This change in particle behavior was further confirmed with imaging of aliquots on cryoSEM for morphology. At later time points, the thrombin-sensitive nanogels displayed more stellate-like morphology, much like active platelet morphology and ULC microgels (**Figure 3**).

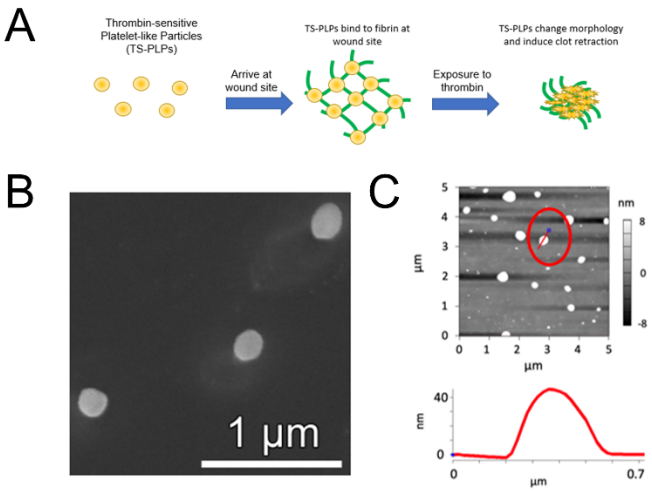

Figure 2: A) Schematic of TS-PLP Function. B) Representative cryoSEM image of TSNs prior to thrombin exposure. When unmodified, TSNs exhibit rounded morphology C) Representative AFM image and height trace of TSNs prior to thrombin exposure.

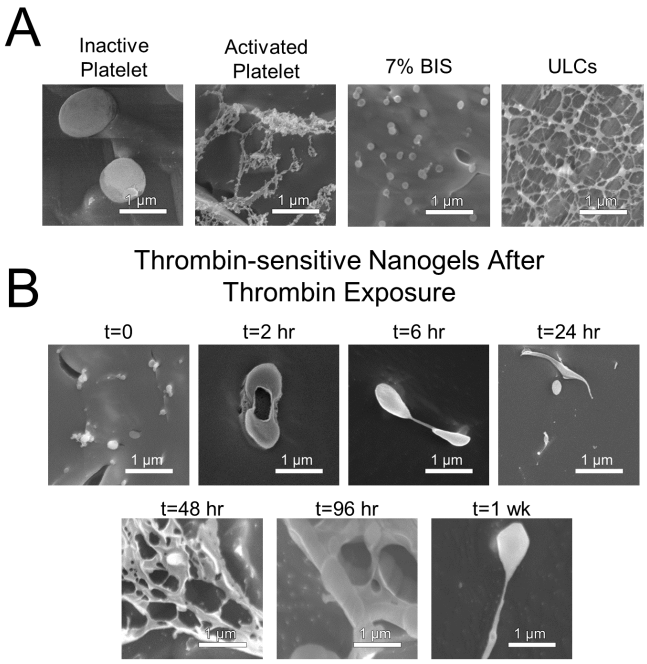

Figure 3: A) Representative cryoSEM images of inactive platelets, activated platelets, and size-matched control 7% BIS crosslinked and ultralow crosslinked (ULC) microgels. Scale bar = 1 µm B) Representative cryoSEM images of thrombin-sensitive nanogels (TSNs) at various time points following exposure to 75 U/mL thrombin.

Thrombin-sensitive Nanogel Loading Behavior: Because NIPMAM does not undergo self-crosslinking, complete degradation of particles was expected (18-21). However, thrombin degradation assays showed that particles did not fully degrade. Thus, loading behavior was investigated to determine if thrombin was successfully penetrating the entirety of the particles. Fluorescent levels were observed to be higher at the edges of nanogels and lower in the center for particles loaded with either 70 kDa FITC-dextran or 66 kDa FITC-BSA (**Supplemental Figures 2 and 3**). This observation indicates that there may be limited penetration into the center of the nanogel, explaining why complete degradation was not observed.

Clot Retraction Analysis: After confirming that the nanogels change deformability in the presence of thrombin, we then sought to evaluate if this was sufficient to induce clot retraction when the particles are coupled to a fibrin-binding antibody. Clots including no particles (control), TS-PLPs, size-matched ULC-PLPs (small ULC-PLPs), size-matched 7% BIS-PLPs (small 7 BIS-PLPs) and ULC-PLPs (corresponding to the size of our original design) were created, with +thrombin counterparts receiving a 100 U/mL thrombin overlay 2 hours after initiation of polymerization. All clots were then imaged on cryoSEM for clot structure **(Figure 4)**. The resulting images were then analyzed for % porosity, which is defined as black pixel area/total image pixels.

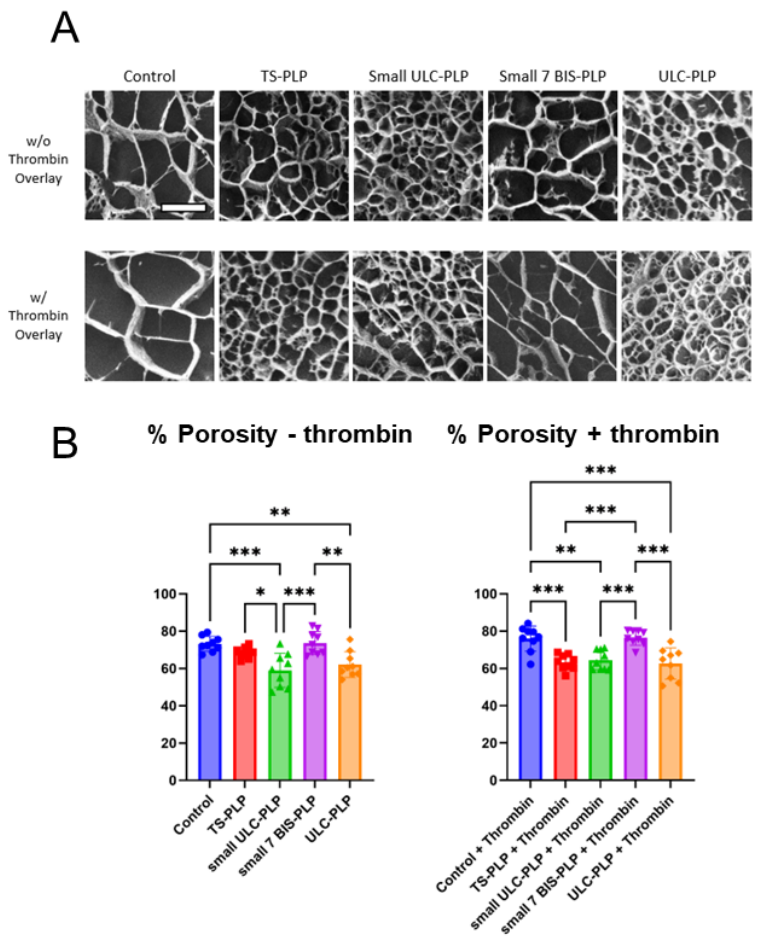

Figure 4: A) Representative cryoSEM images of fibrin clots polymerized in the presence of TS-PLPs, small ULC-PLPs, small 7 BIS-PLPs, and ULC-PLPs. Each image is 30 µm x 30 µm. Scale bar = 10 µm B) Mean percent porosity for each group of clots. Notably, significantly lower percent porosity was observed in small ULC-PLP and ULC-PLP groups in clots with no thrombin overlay but not in clots incorporated with unmodified TS-PLPs. After a thrombin overlay, significantly lower percent porosity was also observed in clots with TS-PLPs incorporated in addition to the ULC-PLP groups. n=9 images per group (3 images per clot, 3 clots per group). One-way ANOVA with Tukey's test was used for all comparisons for data presented in this figure.* = $p \leq 0.05$, ** = $p \leq 0.01$, *** = $p \leq 0.001$

For clots without a thrombin overlay, average % porosity was determined to be 73± 4 for control, 68 ± 3 for TS-PLPs, 59 ± 9 for small ULC-PLPs, 74 ± 6 for small 7 BIS-PLPs, and 62 ± 7 for ULC-PLPs. For clots with a thrombin overlay, average % porosity was determined to be 76 ± 7 for control, 63 ± 4 for TS-PLPs, 64 ± 5 for small ULC-PLPs, 76 ± 4 for small 7 BIS-PLPs, and 63 ± 8 for ULC-PLPs. Without the addition of a thrombin overlay, it was found that clots with

unmodified TS-PLPs incorporated do not have significantly lower % porosity whereas clots with small ULC-PLPs ($p \leq 0.001$) and ULC-PLPs have significantly lower % porosity ($p \leq 0.01$). Thus, the ULC-PLP particle types perform as expected. With the addition of a thrombin overlay, in contrast, clots with TS-PLPs demonstrate a significantly lower % porosity ($p \leq 0.001$), on par with lower % porosity observed in clots with small ULC-PLPs ($p \leq 0.001$) and ULC-PLPs ($p \leq 0.001$).

Analysis of in vivo Hemostasis Following Traumatic Liver Laceration: We next evaluated the hemostatic ability of the TS-PLPs in a survival traumatic liver laceration model. Average blood loss (g blood loss/g animal) was $5.2 \times 10^{-3} \pm 3.1 \times 10^{-3}$ for saline treated animals, $1.3 \times 10^{-3} \pm 0.78 \times 10^{-3}$ for TS-PLP treated animals, $2.0 \times 10^{-3} \pm 0.96 \times 10^{-3}$ for size-matched ULC-PLP treated animals, and $2.8 \times 10^{-3} \pm 1.1 \times 10^{-3}$ for size-matched 7% BIS-PLP treated animals. Average bleeding area was 6.7 ± 2.9 cm^2 for saline treated animals, 1.8 ± 0.7 cm^2 for TS-PLP treated animals, 2.7 ± 1.8 cm^2 for size-matched ULC-PLP treated animals, and 4.0 ± 1.2 cm^2 for size-matched 7% BIS-PLP treated animals. In mice treated with TS-PLPs, significantly lower blood loss and bleeding area were observed compared to saline treated animals. Additionally, TS-PLPs reduce bleeding to a similar extent as ULC-PLPs when comparing blood loss. However, only TS-PLPs resulted in statistically significant lower bleeding area. For bleeding over time, it was found that compared to saline treated mice, TS-PLP treated mice saw significantly reduced blood loss as early as t=1 min and ULC-PLP treated mice saw significantly reduced blood loss as early as t=2 min, potentially suggesting that TS-PLPs stem bleeding sooner. Notably, TS-PLPs maintain similar initial bleeding area rate as ULC-PLPs but then plateaus into lower total bleeding area compared to ULC-PLPs. (**Figure 5B)** Similarly, in an additional cohort of animals in terminal studies, TS-PLPs significantly reduced average blood loss compared to saline controls. (**Supplemental Figure 4**)

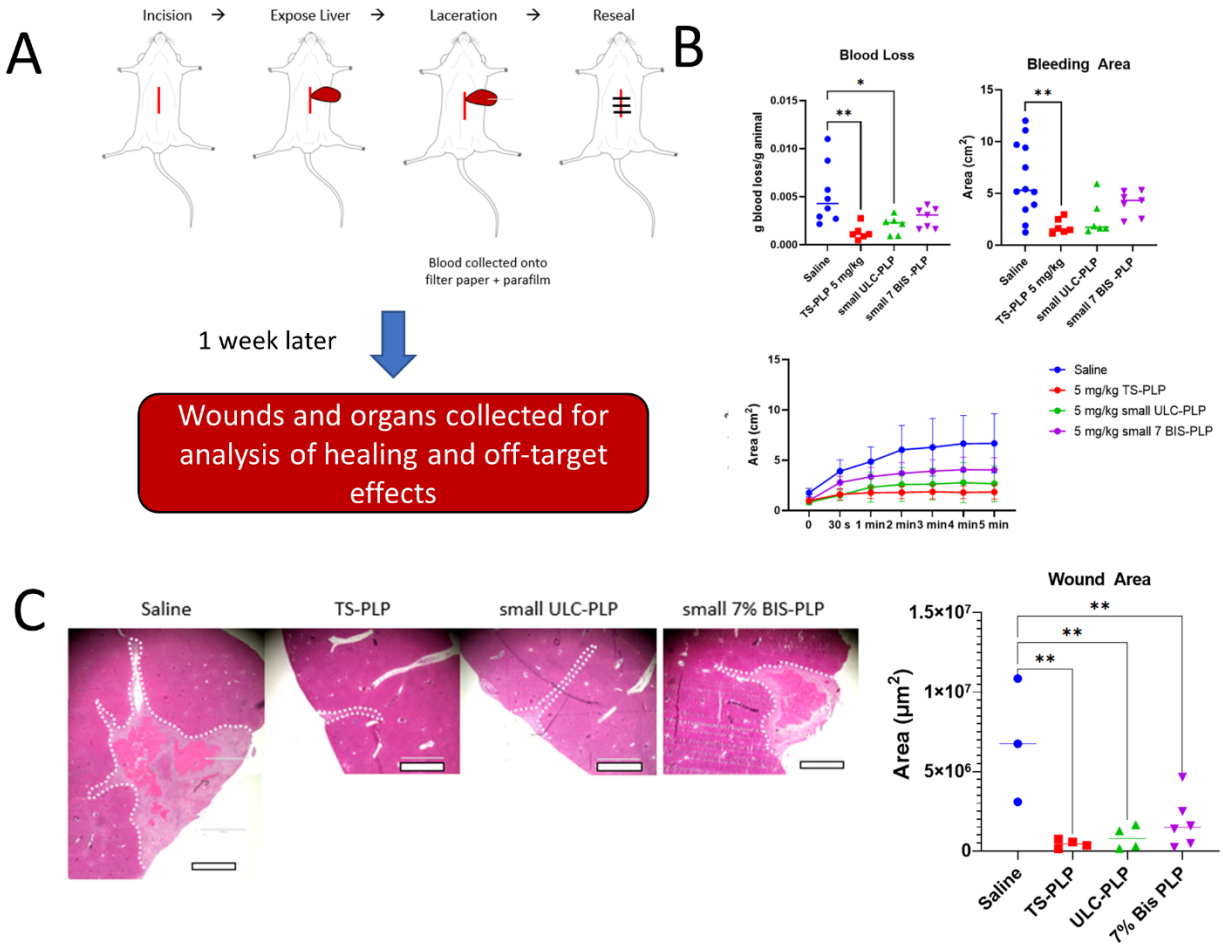

Figure 5: A) Schematic of survival liver laceration model B) Summary of blood loss data. Mice treated with TS-PLPs displayed significantly lower blood loss and bleeding area. Mice treated with TS-PLPs and size-matched ULC-PLPs displayed significant decreases in bleeding compared to control animals. n=6-8 animals per group. C) H&E stained wound sections with summary of wound area measurements. Scale bar = 1000 µm. Mice treated with all hemostatic particles had significantly lower average wound area when compared to saline mice, though the standard deviation was lowest in the TS-PLP group. n=3-6 mice per group. Comparisons were made in bleeding area by non-parametric one-way ANOVA with Dunn's test, comparisons were made in bleeding area vs. time by two-way ANOVA and comparisons were made in all other data by normal one-way ANOVA with Tukey's test.* = $p \leq 0.05$, ** = $p \leq 0.01$, *** = $p \leq 0.001$

Analysis of in vivo Wound Healing Outcomes Following Traumatic Liver Laceration: To evaluate longer term healing outcomes after cessation of bleeding, wound area was measured from H&E stained sections (**Figure 5C**) and fibrin positive area, CD61+ area, and particle presence were measured from immunofluorescent stained sections collected from animals 7 days post-injury **(Figure 6)**. Average wound area was $6.9 \times 10^6 \pm 3.9 \times 10^6$ μm^2 for saline treated animals, $0.5 \times 10^6 \pm 0.3 \times 10^6$ μm^2 for TS-PLP treated animals, $0.8 \times 10^6 \pm 0.7 \times 10^6$ μm^2 for size-matched ULC-PLP treated animals, and $1.8 \times 10^6 \pm 1.6 \times 10^6$ μm^2 for size-matched 7% BIS-PLP treated animals (**Figure 5C**). Average fibrin area was 4585 ± 1417 μm^2 for saline treated animals, 16458 ± 11202 μm^2 for TS-PLP treated animals, 3725 ± 2058 μm^2 for size-matched ULC-PLP treated animals, and 3414 ± 3140 μm^2 for size-matched 7% BIS-PLP treated animals (**Figure 6**). Average CD61+ area was 4762 ± 3353 μm^2 for saline treated animals, 2545 ± 2585 μm^2 for TS-PLP treated animals, 3945 ± 1739 μm^2 for size-matched ULC-PLP treated animals, and 5668 ± 5305 μm^2 for size-matched 7% BIS-PLP treated animals (**Figure 6**). Average particle presence area was 0 μm^2 for all treatment groups (**Figure 6**). In terminal, acute studies, the average fibrin area was 1433 ± 1716 μm^2 for saline treated animals and 2849 ± 2073 μm^2 for TS-PLP treated mice. The average particle presence area in these animals was 35.6 ± 47.41 μm^2 for saline treated animals and 1175 ± 1449 μm^2 in TS-PLP treated mice (**Supplemental Figure 4B**).

Overall, significantly smaller wound areas and CD61+ expression were observed one week after injury in animals treated with TS-PLPs, size-matched ULC-PLPs, and size-matched 7% BIS-PLPs. However, fibrin presence was significantly higher only in animals treated with TS-PLPs. The higher presence of fibrin one week after injury indicates that fibrin-stability is greater *in vivo* in these animals. Additionally, no significant differences were observed in particle presence across all groups, indicating that any particles administered to mice were no longer retained in the injury

site 1week post-injury (**Figure 6**). However, histological analysis of wounds harvested immediately after the bleeding period revealed greater fibrin signal and significantly increased particle signal, indicating TS-PLPs do enhance clot formation, which can subsequently lead to the greater fibrin stability and wound healing observed 1 week post-treatment, and are wound targeting **(Supplemental Figure 4**).

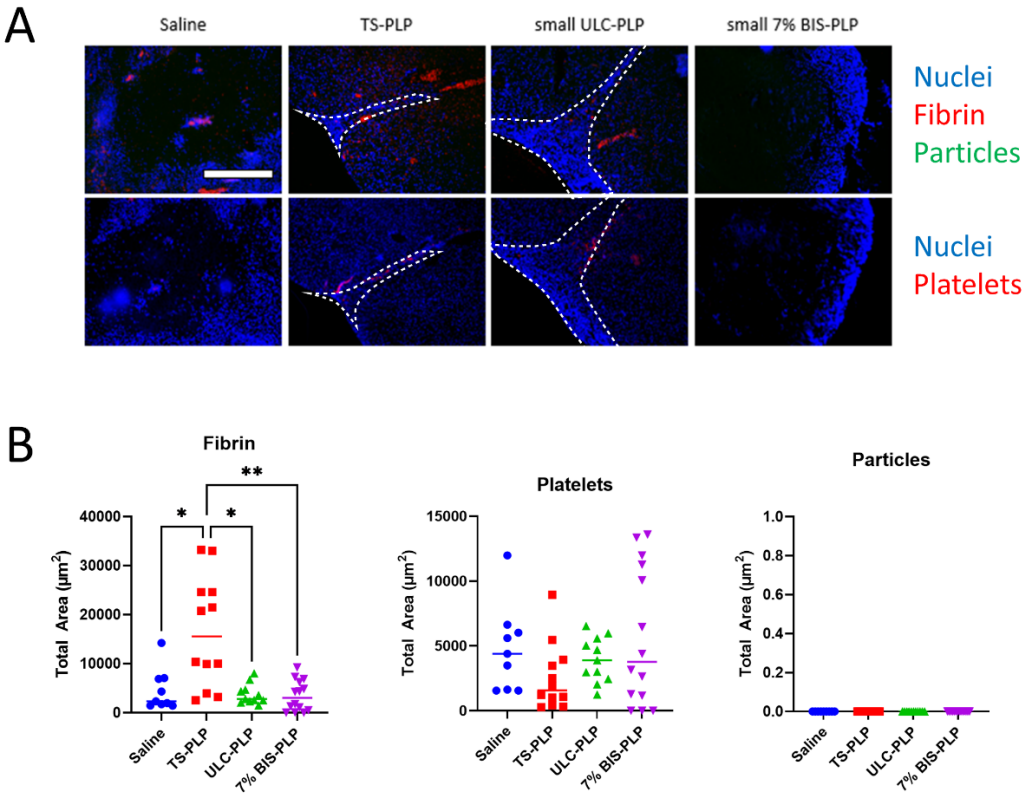

Figure 6: A) Representative IHC wound sections collected 1 week after injury where cell nuclei, fibrin and particles were fluorescently labeled (top row) and cell nuclei and platelets were fluorescently labeled (bottom row). Wound areas are denoted in white. For saline and 7% BIS-PLP treated wounds, the whole image is representative of wound area (due to the much larger sized wound sites in these groups). Scale bar = 400 µm B) Summary of total area of fibrin, particles, and platelet presence (CD61+). Mice treated with TS-PLPs were observed to have significantly higher fibrin presence while there were no significant differences observed in platelet presence and particle presence. Non-parametric one-way ANOVA with Dunn's test was used for comparisons

in all data presented on this figure. n=3 images per wound and 3-5 animals per group. * = $p \leq 0.05$, ** = $p \leq 0.01$

Analysis of Safety and Potential Off-target Effects: To evaluate potential off-target effects, peripheral organs were stained by H&E for tissue morphology and fluorescently labeled for fibrin and particles and measured for fibrin-positive and particle presence areas. Across all organs, tissue morphology appeared normal and no significant differences in fibrin and particle presence were detected when comparing saline-treated mice to TS-PLP and ULC-PLP treated mice. Notably, TS-PLP treated mice tested as having statistically significantly lower particle presence than 7% BIS PLP treated mice in the lung, kidney, and spleen. Interestingly, 7% BIS PLP treated mice also displayed statistically significant lower fibrin presence in the liver compared to saline treated mice. (**Figure 7)**.

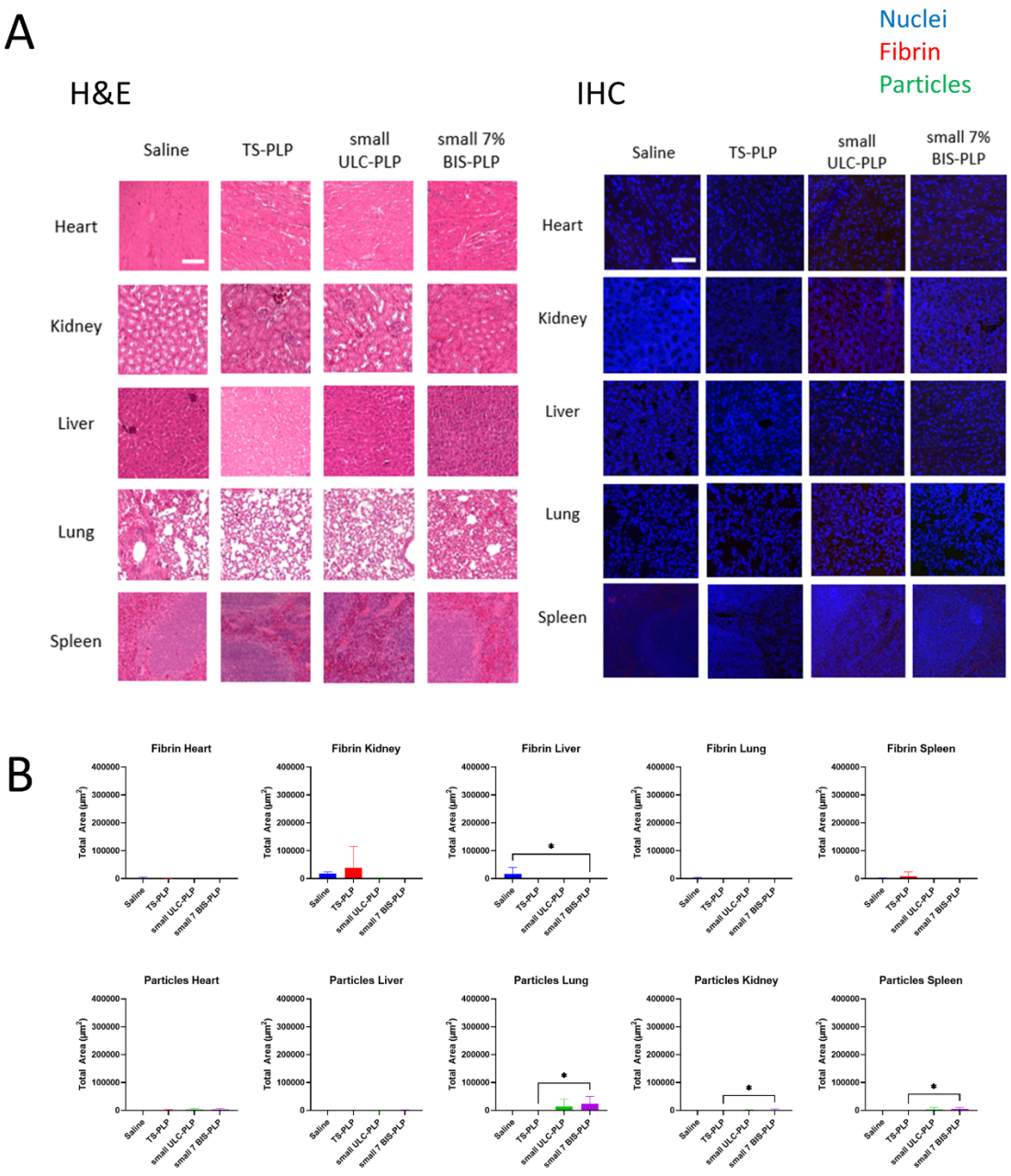

Figure 7: Summary of off-target effects studies. A) Representative images of both H&E to characterize gross tissue morphology and fluorescently labeled peripheral organs for fibrin and particle presence. Images are 400 μm x 400 μm. Scale bar = 100 μm B) Summary of total area for fibrin and particle presence, separated by organ type. Fibrin and particle presence were analyzed by particle analysis in ImageJ. For each organ type, n=3-5 animals were analyzed per group. Overall, compared with saline treated mice, no significant differences in both fibrin and particle presence were observed with relatively low total area detected in the organs of mice treated with TS-PLPs and ULC-PLPs (compared to total area detected in wounds). Non-parametric one-way ANOVA with Dunn's test was used for comparisons made in all data presented in this figure. *= $p \leq 0.05$

Discussion and Conclusions

PLPs are a promising material to address the issues associated with platelet depletion in conditions such as traumatic injury and surgical associated bleeding. Initial PLP designs are capable of homing specifically to injuries and mimic natural platelet clot retraction. However, the original PLP design lacks the natural platelet ability to conditionally change shape after activation of the coagulation cascade. To address this shortcoming, we developed a thrombin-sensitive formulation capable of mimicking wound-induced shape change based on the presence of thrombin. These thrombin-sensitive PLPs (TS-PLPs) can be injected intravenously, home to injury sites, and bind and augment fibrin formation (**Figure 8**). Following exposure to thrombin at the wound site, the TS-peptide is cleaved, resulting in a particle shape change that supports clot retraction and healing. In these studies, we were able to demonstrate that TS-PLPs can induce clot retraction in the presence of thrombin to a similar extent as our first-generation PLP technology while also demonstrating thrombin-triggered shape change (**Figure 8**).

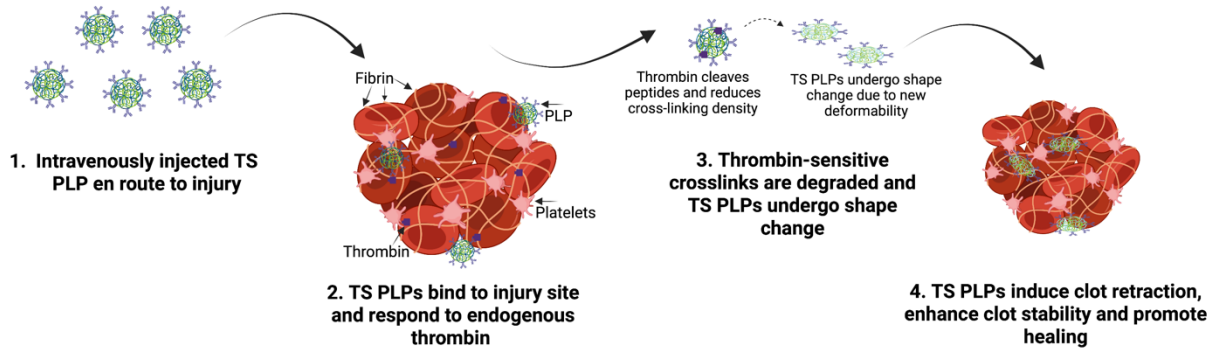

Figure 8: Overview of Thrombin-Sensitive Platelet-like-particle (TS-PLPs) activity.

Prior to exposure to thrombin, TS-PLPs have a rounded shape and do not have significant deformability as indicated by the relatively high particle height, compared to previous findings with ULC-PLPs (16, 23, 24) (**Figure 2**). After exposure to thrombin, TS-PLPs change shape, displaying morphology most like activated platelets and small ULC-PLPs at t=48 hrs (**Figure 3**). Only in this morphology were TS-PLPs capable of significantly retracting the clot structure like ULC-PLPs (**Figure 4**).

Additionally, TS-PLPs demonstrated significant hemostatic ability and wound healing enhancement *in vivo*. In wounds harvested directly after injury, TS-PLPs were visualized at the wound tissue, supporting the claim that PLPs are specific to fibrin present at the injury site. TS-PLPs and ULC-PLPs decreased bleeding significantly compared to control animals treated with saline. Interestingly, 7% BIS-PLPs had a lower mean blood loss and bleeding area than control animals, but bleeding was not significantly different between the two groups. Other studies by our group using larger 7% BIS-PLPs and ULC-PLPs did not demonstrate differences in hemostatic outcomes between these groups but did show differences in clot retraction (15). These results suggest that both particle size and deformability synergistically influence hemostatic outcomes, and this relationship should be studied in more detail in future studies. Additionally, TS-PLPs

demonstrated hemostatic ability to greater statistical significance than size-matched ULC-PLPs when compared to blood loss in mice treated with saline, although direct comparison between TS-PLPs and size-matched ULC-PLPs is not statistically significant. 7 days after injury, significantly lower wound area was observed in injury sites of mice treated with all PLP groups, However, only mice treated with TS-PLPs were observed to have significantly enhanced fibrin presence, potentially indicating greater *in vivo* fibrin stability.

While these studies describe a platelet-mimetic particle that conditionally changes shape in response to wound triggers, to create a more "platelet-like" particle, there are still aspects that could be further optimized. For example, while TS-PLPs do indeed change shape as a result of thrombin exposure, the degradation of crosslinks occur over long time scales. The concentration of thrombin used in our *in vitro* experiments was 50-100 U/mL. The concentration of free thrombin during coagulation is highly variable but has been estimated to vary from 1nM (0.1 U/mL) to higher than 500 nM (25). The local concentration within the wound microenvironment would also be expected to reach even higher concentrations due to rapid local thrombin generation. Therefore, these concentrations are physiologically relevant; however, it is also possible that thrombin levels within clots may be at even higher levels than those tested in our *in vitro* assays and could thus lead to more immediate TS-PLP shape change. Potential future studies should involve further investigation of thrombin-degradation and interaction with TS-PLPs using an even higher range of thrombin concentrations. The rate of degradation could potentially be further enhanced by coupling TS-PLPs to thrombin delivery systems (26). Additionally, it is unknown if the current design allows for retention of thrombin within the microgel for extended periods of time. If this is the case, the microgel may act as a source of thrombin within the wound site for some time after injury. Thus, some other potential directions for future work could entail evaluating these

parameters. Additionally, characterization of particle morphological changes through the use of transmission electron microscopy would further strengthen these findings and will be performed in future studies. Finally, while we have previously shown that PLP-mediated clot retraction increases stiffness *in vitro* (16), we did not characterize increased stiffness of wound tissue *in vivo*. Future studies should more directly investigate the influence of PLPs on wound tissue mechanics *in vivo*.

In conclusion, we were able to successfully fabricate a wound-triggered shape changing PLP with TS-PLPs. As demonstrated in this work, in the absence of thrombin, TS-PLPs display a rounded morphology, similar to inactive platelets. Following exposure to thrombin, TS-PLPs change into a stellate morphology, like active platelets. In this state, TS-PLPs can induce clot retraction to a similar extent as ULC-PLPs. Additionally, TS-PLPs were demonstrated to decrease bleeding and improve wound healing outcomes in a survival liver laceration mouse model. Although further optimization of some aspects is still needed, TS-PLPs, nonetheless, demonstrated promising qualities as a hemostatic and wound healing material.

Acknowledgements: Funding was provided by the National Science Foundation DMR CAREER 1847488 (ACB) and NSF GFRP to SP. This work was performed in part at the Analytical Instrumentation Facility (AIF) at North Carolina State University, which is supported by the State of North Carolina and the National Science Foundation (award number ECCS-2025064). The AIF is a member of the North Carolina Research Triangle Nanotechnology Network (RTNN), a site in the National Nanotechnology Coordinated Infrastructure (NNCI). The authors acknowledge the use of the Cellular and Molecular Imaging Facility (CMIF) at North Carolina State University, which is supported by the State of North Carolina and the National Science Foundation. Biorender was used to create Figures 1, 2, and 8.

Conflict of Interest Statement: Ashley Brown is Co-Founder of Selsym Biotech, Inc., a start-up company focused on developing injectable hemostatic therapeutics. Other authors have no disclosures.

Data Availability Statement: The data that support the findings of this study are available from the corresponding author upon reasonable request.

Ethics Approval Statement: All animal studies were approved by the NC State IACUC.

References

1. Jansen EE, Hartmann M. Clot Retraction: Cellular Mechanisms and Inhibitors, Measuring Methods, and Clinical Implications. Biomedicines. 2021;9(8). Epub 2021/08/28. doi: 10.3390/biomedicines9081064. PubMed PMID: 34440268; PMCID: PMC8394358.
2. Nurden AT. Molecular basis of clot retraction and its role in wound healing. Thromb Res. 2022. Epub 2022/08/26. doi: 10.1016/j.thromres.2022.08.010. PubMed PMID: 36008192.
3. Kutcher ME, Redick BJ, McCreery RC, Crane IM, Greenberg MD, Cachola LM, Nelson MF, Cohen MJ. Characterization of platelet dysfunction after trauma. J Trauma Acute Care Surg. 2012;73(1):13-9. Epub 2012/06/30. doi: 10.1097/TA.0b013e318256deab. PubMed PMID: 22743367; PMCID: PMC3387387.
4. Ten leading causes of death and injury. Centers for Disease Control and Prevention Web site. [updated 2019; cited 2019 Dec 9]. Available from: https://www.cdc.gov/injury/wisqars/LeadingCauses.html.
5. National diabetes statistics report. Center for Disease Control and Prevention Web site. 2020 [updated 2020; cited 2020 June 9]. Available from: https://www.cdc.gov/diabetes/data/statistics/statistics-report.html. .
6. Davidow EB, Brainard B, Martin LG, Beal MW, Bode A, Ford MJ, Ramsey N, Fagella A, Jutkowitz A. Use of fresh platelet concentrate or lyophilized platelets in thrombocytopenic dogs with clinical signs of hemorrhage: a preliminary trial in 37 dogs. Journal of Veterinary Emergency and Critical Care. 2012;22(1):116-25. doi: 10.1111/j.1476-4431.2011.00710.x.
7. Hux BD, Martin LG. Platelet transfusions: treatment options for hemorrhage secondary to thrombocytopenia. Journal of Veterinary Emergency and Critical Care. 2012;22(1):73-80. doi: 10.1111/j.1476-4431.2011.00706.x.
8. Modery-Pawlowski CL, Tian LL, Ravikumar M, Wong TL, Gupta AS. In vitro and in vivo hemostatic capabilities of a functionally integrated platelet-mimetic liposomal nanoconstruct. Biomaterials. 2013;34(12):3031-41. doi: 10.1016/j.biomaterials.2012.12.045.
9. Ponschab M, Schlimp CJ, Zipperle J, Gabriel C, Süssner S, Cadamuro J, Gratz J, Redl H, Schöchl H. Platelet function in reconstituted whole blood variants. Journal of Trauma and Acute Care Surgery. 2015;79(5):797-804. doi: 10.1097/ta.0000000000000852.
10. Gaston E, Fraser JF, Xu ZP, Ta HT. Nano- and micro-materials in the treatment of internal bleeding and uncontrolled hemorrhage. Nanomedicine: Nanotechnology, Biology and Medicine. 2018;14(2):507-19. doi: 10.1016/j.nano.2017.11.007.

11. Girish A, Sekhon U, Sen Gupta A. Bioinspired artificial platelets for transfusion applications in traumatic hemorrhage. Transfusion. 2019;60(2):229-31. doi: 10.1111/trf.15543.
12. Nandi S, Brown AC. Platelet-mimetic strategies for modulating the wound environment and inflammatory responses. Exp Biol Med (Maywood). 2016;241(10):1138-48. Epub 2016/05/18. doi: 10.1177/1535370216647126. PubMed PMID: 27190260; PMCID: PMC4950360.
13. Nellenbach K, Brown AC. Platelet-mimicking procoagulant nanoparticles: Potential strategies for mitigating blood shortages. Journal of Thrombosis and Haemostasis. 2022;20(8):1756-8. doi: 10.1111/jth.15720.
14. Greineder CF, Brenza JB, Carnemolla R, Zaitsev S, Hood ED, Pan DC, Ding B-S, Esmon CT, Chacko AM, Muzykantov VR. Dual targeting of therapeutics to endothelial cells: collaborative enhancement of delivery and effect. The FASEB Journal. 2015;29(8):3483-92. doi: 10.1096/fj.15-271213.
15. Brown AC, Stabenfeldt SE, Ahn B, Hannan RT, Dhada KS, Herman ES, Stefanelli V, Guzzetta N, Alexeev A, Lam WA, Lyon LA, Barker TH. Ultrasoft microgels displaying emergent platelet-like behaviours. Nat Mater. 2014;13(12):1108-14. Epub 2014/09/10. doi: 10.1038/nmat4066. PubMed PMID: 25194701; PMCID: PMC4239187.
16. Nandi S, Sproul EP, Nellenbach K, Erb M, Gaffney L, Freytes DO, Brown AC. Platelet-like particles dynamically stiffen fibrin matrices and improve wound healing outcomes. Biomater Sci. 2019;7(2):669-82. Epub 2019/01/05. doi: 10.1039/c8bm01201f. PubMed PMID: 30608063; PMCID: PMC6385160.
17. Sproul EP, Nandi S, Roosa C, Schreck L, Brown AC. Biomimetic microgels with controllable deformability improve healing outcomes. Adv Biosyst. 2018;2(10). Epub 2018/10/01. doi: 10.1002/adbi.201800042. PubMed PMID: 33564714; PMCID: PMC7869964.
18. Clarke KC, Dunham SN, Lyon LA. Core/Shell Microgels Decouple the pH and Temperature Responsivities of Microgel Films. Chemistry of Materials. 2015;27(4):1391-6. doi: 10.1021/cm504649t.
19. Gaulding JC, South AB, Lyon LA. Hydrolytically degradable shells on thermoresponsive microgels. Colloid and Polymer Science. 2012;291(1):99-107. doi: 10.1007/s00396-012-2692-0.
20. Smith MH, South AB, Gaulding JC, Lyon LA. Monitoring the erosion of hydrolytically-degradable nanogels via multiangle light scattering coupled to asymmetrical flow field-flow fractionation. Anal Chem. 2010;82(2):523-30. Epub 2009/12/17. doi: 10.1021/ac901725m. PubMed PMID: 20000662; PMCID: PMC2810709.
21. South AB, Lyon LA. Direct Observation of Microgel Erosion via in-Liquid Atomic Force Microscopy. Chemistry of Materials. 2010;22(10):3300-6. doi: 10.1021/cm100702p.
22. Du H, Li C, Luan Y, Liu Q, Yang W, Yu Q, Li D, Brash JL, Chen H. An antithrombotic hydrogel with thrombin-responsive fibrinolytic activity: breaking down the clot as it forms. Materials Horizons. 2016;3(6):556-62. doi: 10.1039/c6mh00307a.
23. Bachman H, Brown AC, Clarke KC, Dhada KS, Douglas A, Hansen CE, Herman E, Hyatt JS, Kodlekere P, Meng Z, Saxena S, Spears Jr MW, Welsch N, Lyon LA. Ultrasoft, highly deformable microgels. Soft Matter. 2015;11(10):2018-28. doi: 10.1039/c5sm00047e.
24. Sproul EP, Nandi S, Chee E, Sivadanam S, Igo BJ, Schreck L, Brown AC. Development of Biomimetic Antimicrobial Platelet-Like Particles Comprised of Microgel Nanogold Composites. Regenerative Engineering and Translational Medicine. 2019;6(3):299-309. doi: 10.1007/s40883-019-00121-6.

25. Wolberg, A, Campbell, R. Thrombin Generation, Fibrin Clot Formation and Hemostasis. Transfus Apher Sci. 2008; 38 (1): 15-23. doi: 10.1016/j.transci.2007.12.005.
26. Sen Gupta A, Girish A, Jolly K, de la Fuente M, Han X, Nieman MT, Recchione A. Intravenous Nanomedicine for Targeted Delivery of Thrombin to Augment Hemostasis. Blood. 2021;138(Supplement 1):1029-. doi: 10.1182/blood-2021-153708.